Bio-mimetic flow control for drag reduction on a three-dimensional model vehicle

Hoon Lee
School of Mechanical and Aerospace Engineering
Seoul National University

Abstract

In the present study, we present a bio-mimetic flow control device for reduction of drag on a model vehicle. The model vehicle from GM company (GM model) is chosen as the base configuration, having various base slant inclination ($\theta = 0^\circ \sim 90^\circ$). This model has the critical slant angle of $\theta = 25^\circ$, at which the drag coefficient is high ($C_D = 0.311$) and the wake structure is very complex. The present device is inspired by secondary feathers of a bird which passively pop up at landing, and is installed at the critical angle to reduce the drag on the model vehicle. The drag on the GM model is decreased by up to 7.5% with the present control device. It is shown that the present device moves the separation point to further downstream, resulting in the base pressure recovery.

Keywords: 3-D vehicle, drag reduction, flow control, bio-mimetic

Student number: 2010-24070

Contents

List of Figures

List of Tables

Table

Nomenclature

Roman Symbols

C_D	drag coefficient
C_{D_p}	pressure drag coefficient
C_{p_f}	pressure coefficient on the frontal area of the model vehicle
C_{p_b}	pressure coefficient on the base area of the model vehicle
G	ground clearance
H	height of the model vehicle
h	length of the flow control device
L	length of the model vehicle
l	length of the additional slant part
Re_H	Reynolds number, $Re = U_0 H/\nu$
U_0	free-stream velocity
u	streamwise velocity
W	width of the model vehicle
x, y, z	Cartesian coordinate

Greek Symbols

δ	boundary layer thickness
δ^*	displacement thickness
θ	slant angle
ν	kinematic viscosity
ω	vorticity

Chapter 1

Introduction

The current energy issue increases the need for aerodynamic drag reduction of the ground vehicles to minimize fuel consumption. In the statistics, a 40% of drag reduction in the ground vehicles would result in 16% of fuel saving in automobile industry Howard & Goodman (1985). Moreover, it is known that a conventional truck whose drag coefficient is 0.6 consumes 65% of its total fuel to resist aerodynamic drag at the speed of 110 km/h. If the drag coefficient of the truck is reduced from 0.6 to 0.5, 10% of fuel will be saved (McCallen *et al.* (1999), figure 1.1). Thus reducing aerodynamic drag on the ground vehicles is one of the most effective way for fuel saving.

The aerodynamic force on the vehicle is closely related to the flow characteristics in the wake and thus many researchers have investigated the flow behind the vehicle. Ahmed (1981) studied the flow around three types of automobile shapes; fastback, notch-back and square-back (estate), as shown in figure 1.2. He observed that the near wake of three different models is characterized by a separation bubble formed by a recirculation region. He also found a pair of longitudinal vortices formed on lateral edges of the roof. Among the models, the fastback had the lowest drag. To focus on the flow around the rear part of a fastback model, Ahmed*et al.* (1984) defined a simplified quarter-scale model vehicle, called Ahmed body (figure 1.3). Ahmed*et al.* (1984) studied the effect of the base slant inclination on the model drag coefficient (figure 1.3) and on the

flow topology. From 0° to 12.5°, the flow remains attached on the slant surface and separates at the rear end base, resulting in a typical square-back wake flow, as described by Khalighi*et al.* (2001). With the increase in the slant angle, a separation bubble and two longitudinal vortices coexist on the slant surface. These flow structures wrestle each other, causing significant pressure drop and resulting in the increase of drag. At a 30° angle, a drag is suddenly decreased. This angle is defined as the critical angle that represents the boundary of the flow modification. After a 30° angle, the influence of the separation becomes bigger and the flow dominated by the vortices evolves to another, closer to a square-back flow, similar to the flow for low slant angles. Through multi-hole pressure tabs, Ahmed*et al.* (1984) also showed that almost 85% of the total drag is the pressure drag.

The flow modification depending on the slant angle suggested by Ahmed*et al.* (1984) is supported by many authors, in particular around the critical slant angle. Lienhart*et al.* (2003) provided a large characterization of the flow around the Ahmed body having 25° and 35° slant angles with laser Doppler velocimetry (LDV) and constant temperature anemometry (CTA) measurements. This study gives an important velocity data base to validate computational fluid dynamics turbulence models for the automotive domain. Spohn & Gillieron (2002) studied the flow modification much more thoroughly than the previous analysis of Ahmed*et al.* (1984) using visualization techniques within a water tunnel. Conan*et al.* (2010) reproduced as closely as possible the reference study of Ahmed*et al.* (1984), and gave detailed explanation of the flow characteristics using particle image velocimetry and coupling oil visualization.

In addition, many flow control strategies around the Ahmed body, or close geometries, have been investigated. Gillieron & Kourta (2010) used splitting plates at the rear end of the Ahmed body. Bruneau & Mortazavi (2008) nu-

merically studied the effect of porous layer on the different model surfaces. Aider*et al.* (2009) examined vortex generators on the roof of the Ahmed body. Beaudoin & Aider (2008) studied the use of flaps on the different edges of the rear part of the Ahmed body. Fourrie*et al.* (2011) investigated the fixed deflector that weakens the vortices by conducting Stereoscopic PIV measurements.

Despite of the efforts to reduce the aerodynamic drag, as mentioned before, it is still hard to applying these control devices to the real vehicle situation (Ortega*et al.* (2009); Mohamed-Kassim & Filippone (2010)). Recently, successful flow control methods have been suggested from bio-mimetic approaches. For example, the riblet is one of the best control methods for friction drag reduction inspired by shark skin, showing maximum 8 % drag reduction (Walsh (1982); Choi*et al.* (1993)). Birds also have an excellent skill to deal with separation on their wing (Liebe (1979)). Once separation starts to develop on the trailing edge of the wing, reversed flow occurs in the separation regime. Responding to the reversed flow, light secondary feathers pop up, as shown in figure 1.4. The feathers prevent further proliferation of flow separation and delay the separation point to downstream. The concept of these pop-up feathers may be applied to the control of flow over a ground vehicle because the delay of separation is an important control strategy for drag reduction on a bluff body (Choi*et al.* (2008)).

In this study, we present a new bio-mimetic flow control device inspired by the secondary feathers of birds. The device is attached to the rear edge of the model vehicle. When the separation occurs on the slant surface, it passively floats under the reversed flow. The mechanism of the device is investigated from the base pressure measurement and velocity measurement using particle image velocimetry.

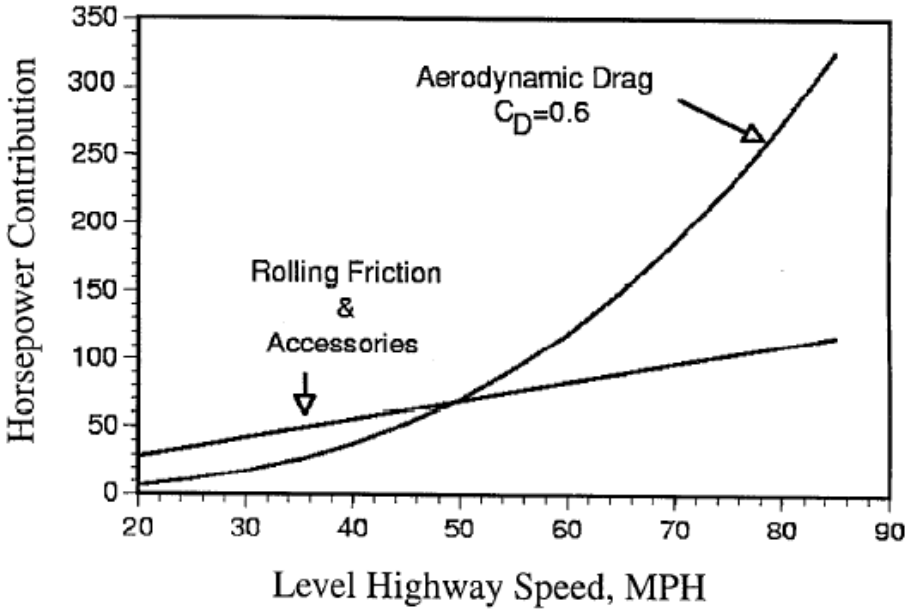

Figure 1.1. Horsepower required to overcome aerodynamic drag and rolling friction/accessories as a function of travel speed for a typical Class 8 tractor-trailer.

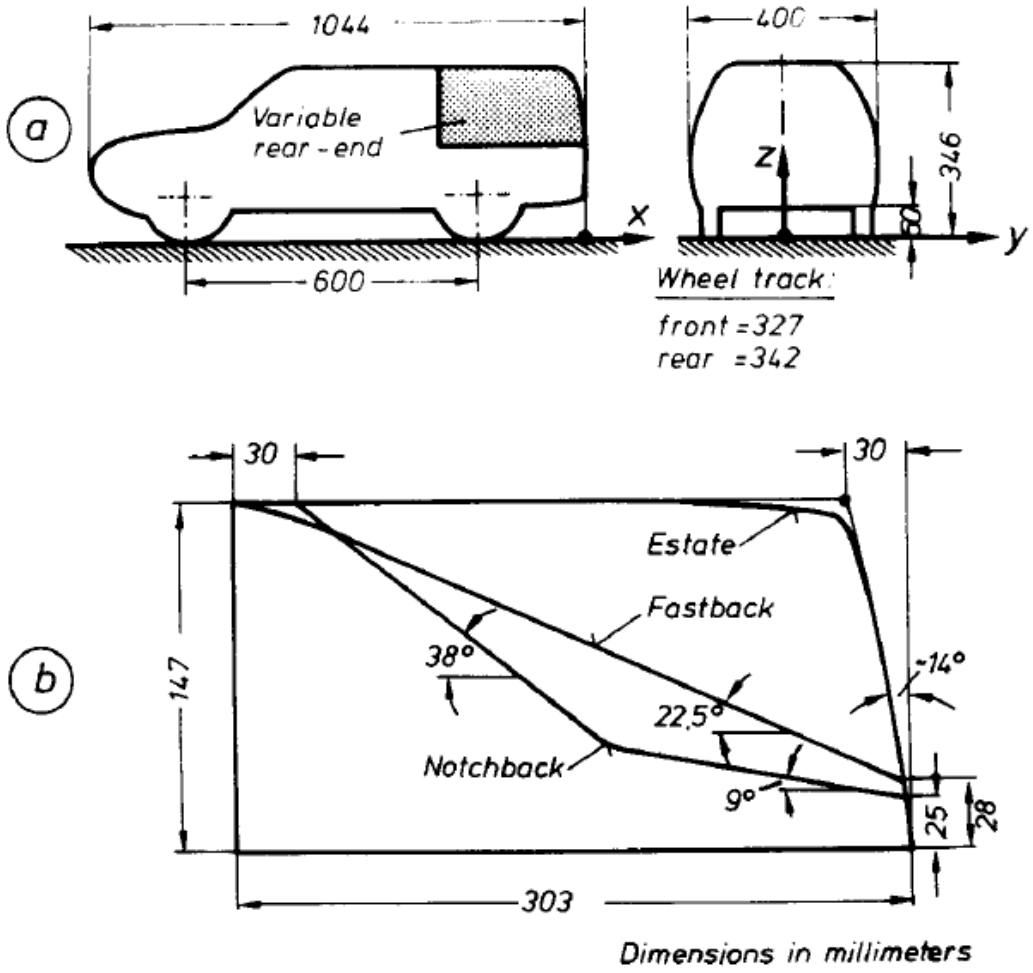

Figure 1.2. Interchangeable rear ends; fastback, notch-back and square-back (estate).

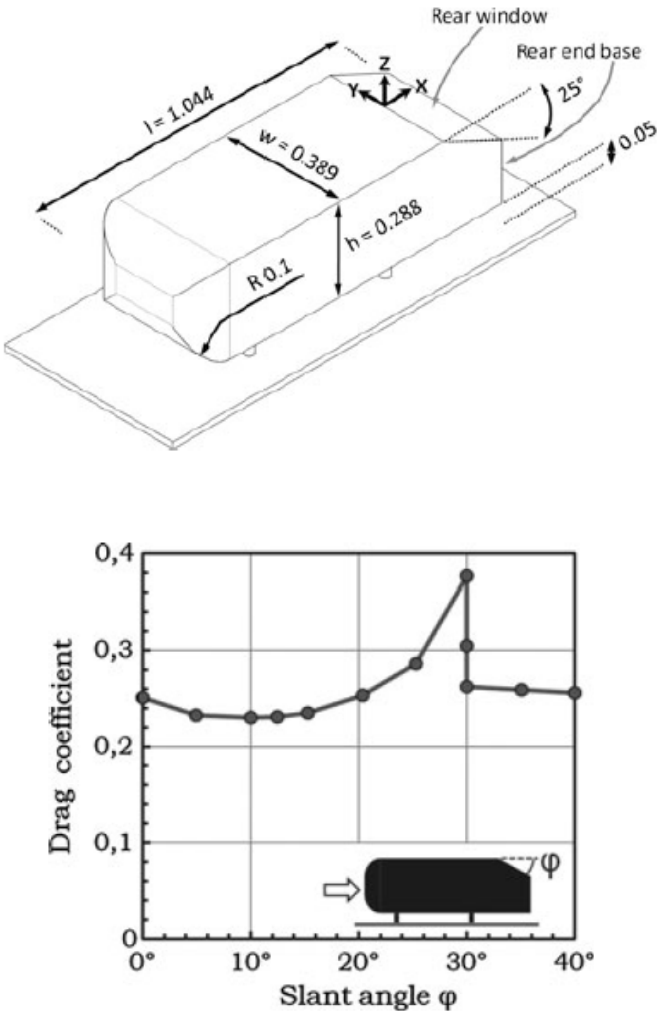

Figure 1.3. The geometry of the Ahmed body, and drag coefficient versus the slant angle.

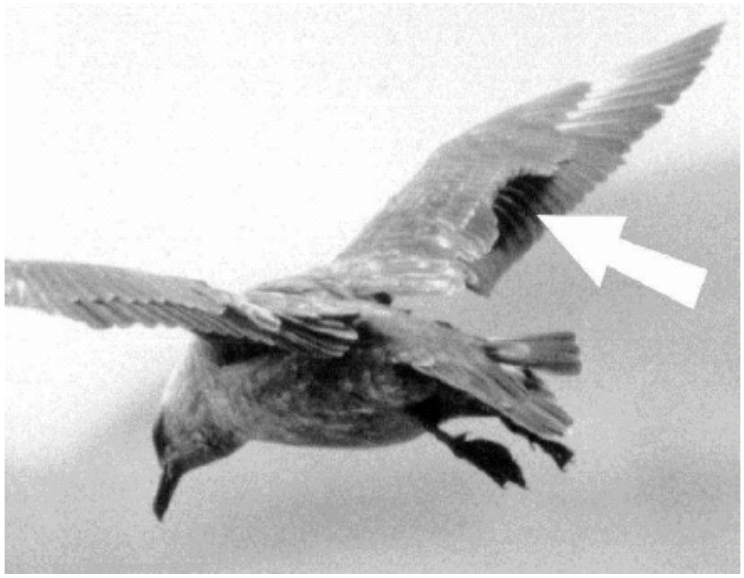

Figure 1.4. The popped up feathers on the wing of a bird.

Chapter 2

Experimental setup

2.1 Model vehicle

The model vehicle used in this study is a modified GM model, by adding a slant part at the base of the original model. The original GM model is a prototype of General Motors (GM) and has been studied by many previous researchers (Han*et al.* (1996); Khalighi*et al.* (2001); Verzicco*et al.* (2002)). It is well known that the model is square-back model and flow field behind the model is characterized by a large recirculation region due to flow separation. The model is made by ABS (acrylonitrile, butadiene and styrene) resin which has excellent characteristics of formability, stiffness, thermal resistance and surface treatment.

For applying the new control device to various model cases and estimating the effectiveness of the device thoroughly, the original model should be modified because the model is only applied to square-back case, such as heavy trucks. Like Ahmed*et al.* (1984) created interchangeable rear-ends to investigate the characteristics of three different car shapes (notch-back, fastback and square-back), the additional slant part is made in this study (figure 2.1). The slant part has various slant angles from 0° to 35°. The step of the slant angle is 5°. The slant part is made by acrylic having many pressure tabs to measure base pressure.

The present model consists of a fore body, a mid-section and the additional slant part. The model is 360 mm long, 140 mm wide and 100 mm high. The distance between the model and the ground is 20 mm. The length of the fore body is 70 mm and the mid-section with rectangular cross section is 290 mm long. The fore body is rounded elliptically in the four surfaces. The leading edge of the fore body has a small rectangular shape of 80×40 mm^2.

2.2 New control device

In this study, the new bio-mimetic flow control device inspired by the secondary feathers of birds is introduced. The device is attached to the rear edge of the model vehicle, as shown in figure 2.2. The device is made of strawboard such that it quickly responds to the flow, like real feathers. Figure 2.3 shows how the device works. The device remains attached at low wind speed because separation does not occur. Once the separation starts to develop on the slant surface, however, the device passively lifts responding to the reversed flow. The device is a tool of passive flow control meaning that no external energy required by the control mechanism. The device self-adjusts to a position dependant on the aerodynamic forces and the device weight. Thus, we call this movable deflector to PMD (passively moving deflector), hereafter. Figure 2.4 shows a configuration of the PMD. It is 140 mm wide and 0.8 mm thick. The length of the PMD (h) varies from 10 mm to 34 mm. 34 mm is the maximum length because the length of the slant surface is about 34 mm. The PMD is attached to a certain slant angle and many measurements are performed. These results will be discussed later.

2.3 Force and base pressure measurements

The force and base pressure measurements are conducted in an open-circuit blowing type wind tunnel at $Re_H = 1.3 \times 10^5$ and $Re_H = 2.0 \times 10^5$ ($U_0 = 20$ and 30 m/s, respectively) based on the height of the model vehicle. Figure 2.5 shows the schematic diagram of the force measurement system in the wind tunnel. The wind tunnel has a test section that is 1500 mm long with 600×600 mm^2 square cross section. All the walls of the test section are made of transparent acrylic plate. Velocity can be controlled up to 30 m/s. The blockage ratio is 3.9% and the turbulent intensity is about 0.5% at the $U_0 = 10$ m/s.

Because vehicles are moving on the ground, boundary layer effect should be minimized. The incoming boundary layer thickness is 12 mm ($\delta/G = 0.6$) at $U_0 = 30$m/s without the model vehicle, measured by hot-wire anemometry (figure 2.6). Using numerical equations, displacement thickness is calculated that $\delta^*/G = 0.085$. It is known that as long as the displacement thickness of the floor boundary layer, as measured in an empty test section, is less than 10% of the vehicle's ground clearance, fixed ground condition (the model vehicle is just fixed on the ground) is adequate for passenger-car development (Hucho & sovran (1993)). In this case, the displacement thickness is smaller than 10% of the ground clearance, $\delta^* = 0.085 \leq 0.1$, thus the effect of boundary layer is negligible.

The time-averaged drag on the model vehicle is measured using an one-axis load cell (CAS, BCL-3L), as shown in (figure 2.7). The load cell is directly connected to the center point of the model mass to minimize the effect of torque. Because the signal produced by the load cell is made of a very low voltage, amplifier is used by 1000 times. By conducting calibration using weights and pulley, the linearity between the voltage and the drag is verified. The maximum

relative uncertainty of the drag is within 1%.

62 pressure taps are located on the base (28 on the slant surface and 34 on the base region). The pressure taps are connected with a digital manometer (MKS 220D) having the measurement range of $0 \sim 10$ Torr. At each measurement point, the pressure is measured for 150 s to obtain a fully converged mean pressure value. Based on 62 pressure data, the pressure contours are drawn using two-dimensional interpolation based on DACE (Design and Analysis of Computer Experiments) that is a Matlab toolbox for working with kriging approximations to computer models.

2.4 Velocity measurement

Velocity measurements are conducted in closed type wind tunnel at $Re = 1.3 \times 10^5$ using a PIV (particle image velocimetry) system, as shown in figure 2.8 and figure 2.9. The test section is 4000 mm long with a 900×900 mm^2 square cross section. To minimize the boundary layer effect, the floor is raised for 340 mm above the ground. The boundary layer thickness on the raised floor is less than 10 mm, thus the effect of boundary layer is also negligible (Hucho & sovran (1993)). The uniformity of the mean stream-wise velocity and the turbulent intensity are both within 0.3 % at 20 m/s. fig shows the field of views that the measurements are taken in vertical center plane (xy-plane) and horizontal plane (xz-plane). These measurements allow the study of a three-dimensional wake structure. The light sheets are provided by a double-pulsed Nd-YAG laser operating at 532 nm, with a 7.25 Hz frequency. The delay between the two pulses is fixed by delay generator, so that particles move from about a fourth of the interrogation window during this delay. The CCD camera size is 2048×2048 pixels^2, the measured field size is 157×157 mm^2 and 146×146

mm^2, in the vertical and the horizontal plane, respectively. The interrogation window is 32×32 $pixels^2$ with 50 % overlapped images, so the spatial resolution is 2.45 mm. Time-averaged fields are obtained from 2000 instantaneous fields. The flow seeding is made by a fog generator.

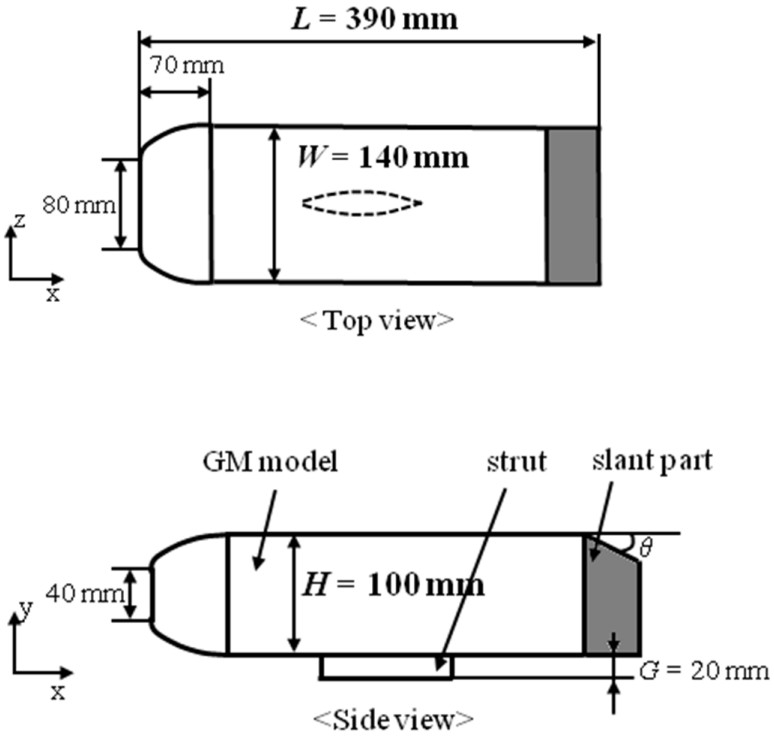

Figure 2.1. The geometry of the GM model.

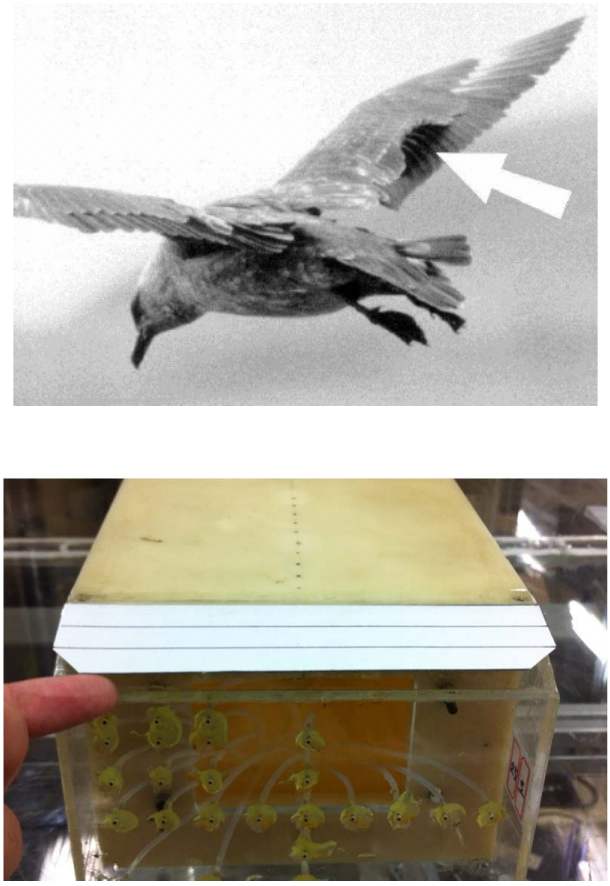

Figure 2.2. The new control device, PMD, motivated by the feather of a bird.

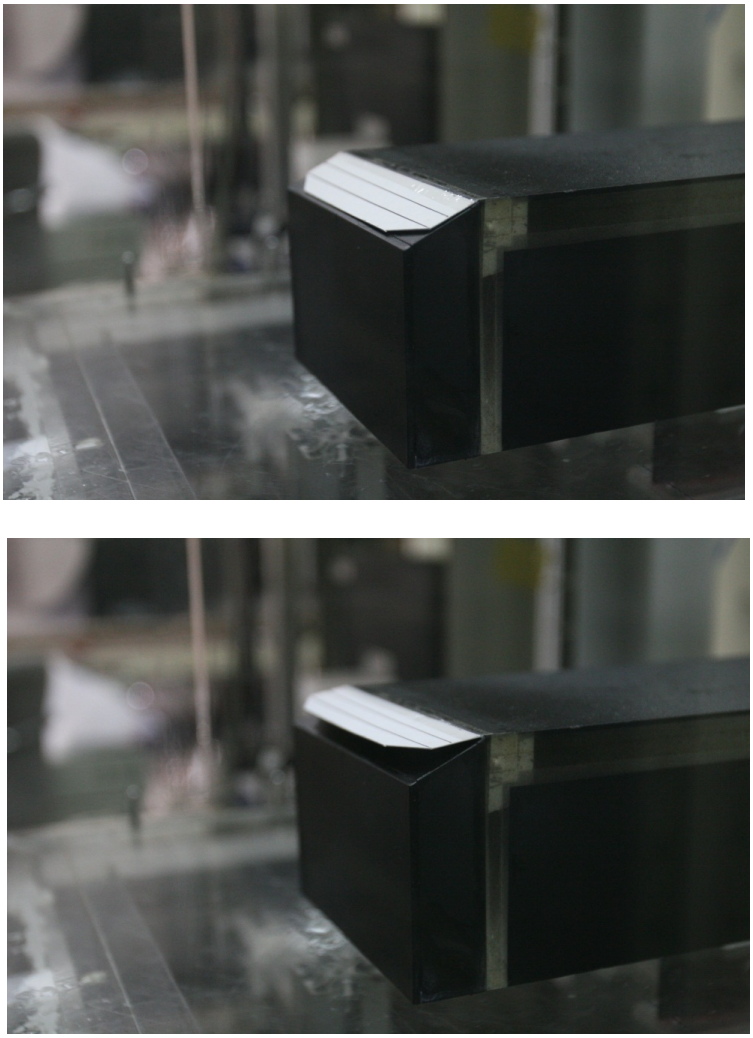

Figure 2.3. Self-lifting PMD.

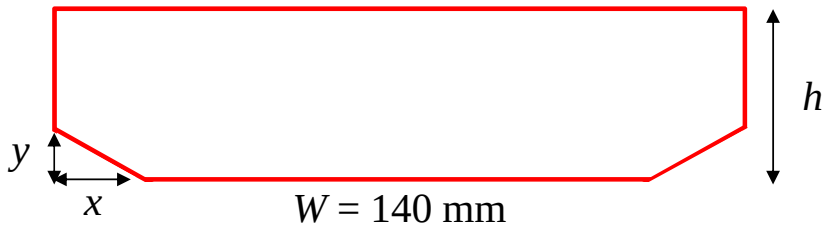

Figure 2.4. The configuration of PMD.

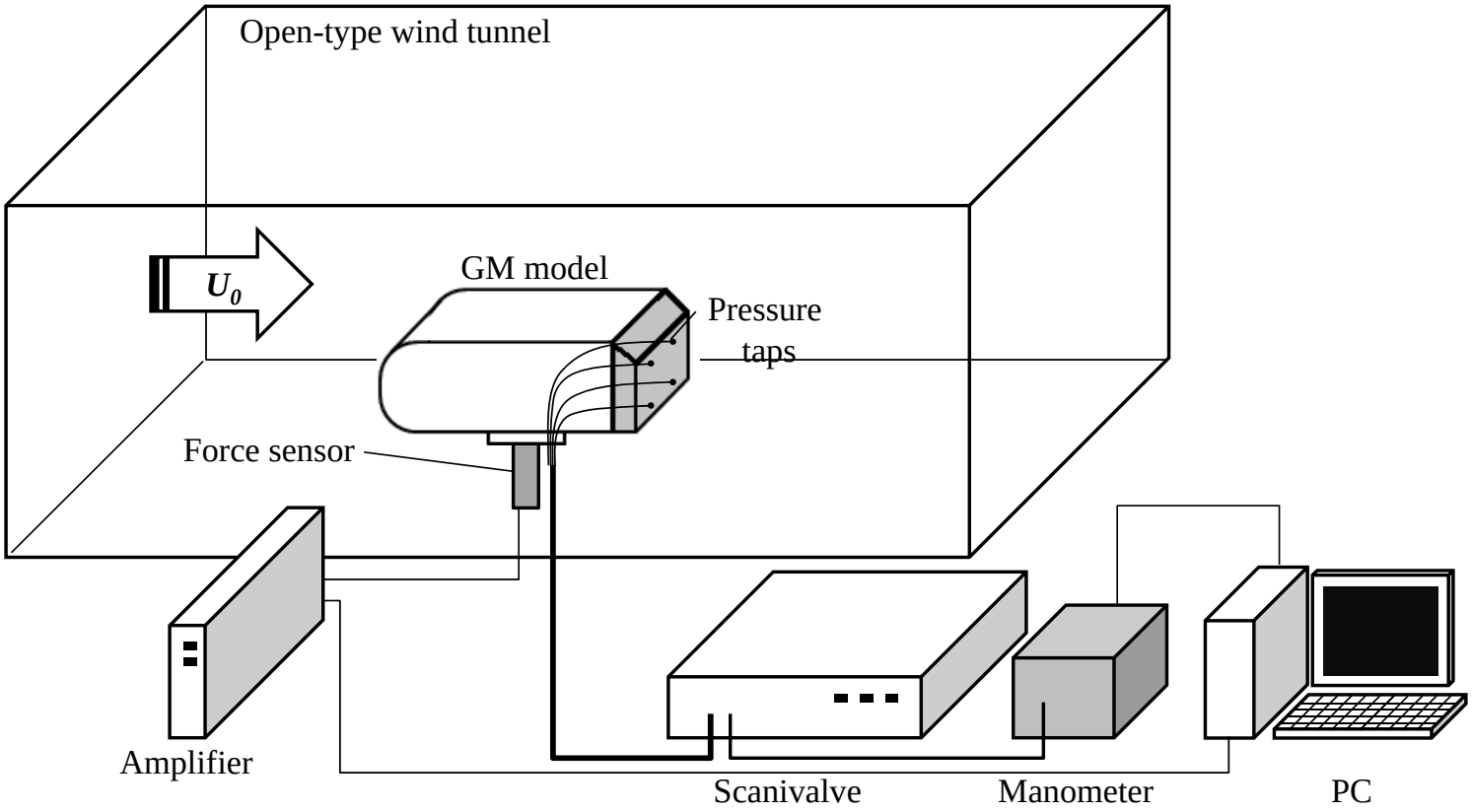

Figure 2.5. The schematic diagram of the force and base pressure measurements system.

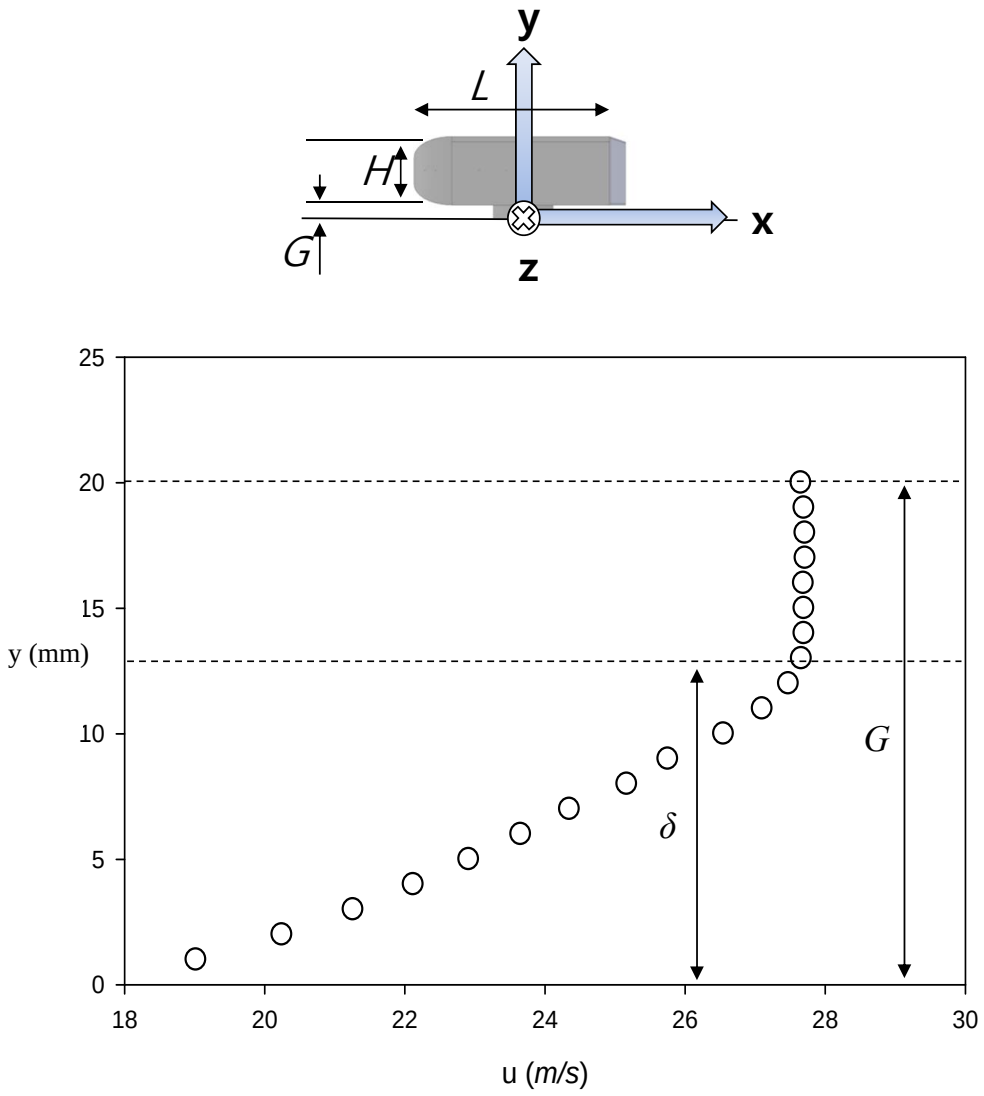

Figure 2.6. The profile of stream-wise velocity close to the ground.

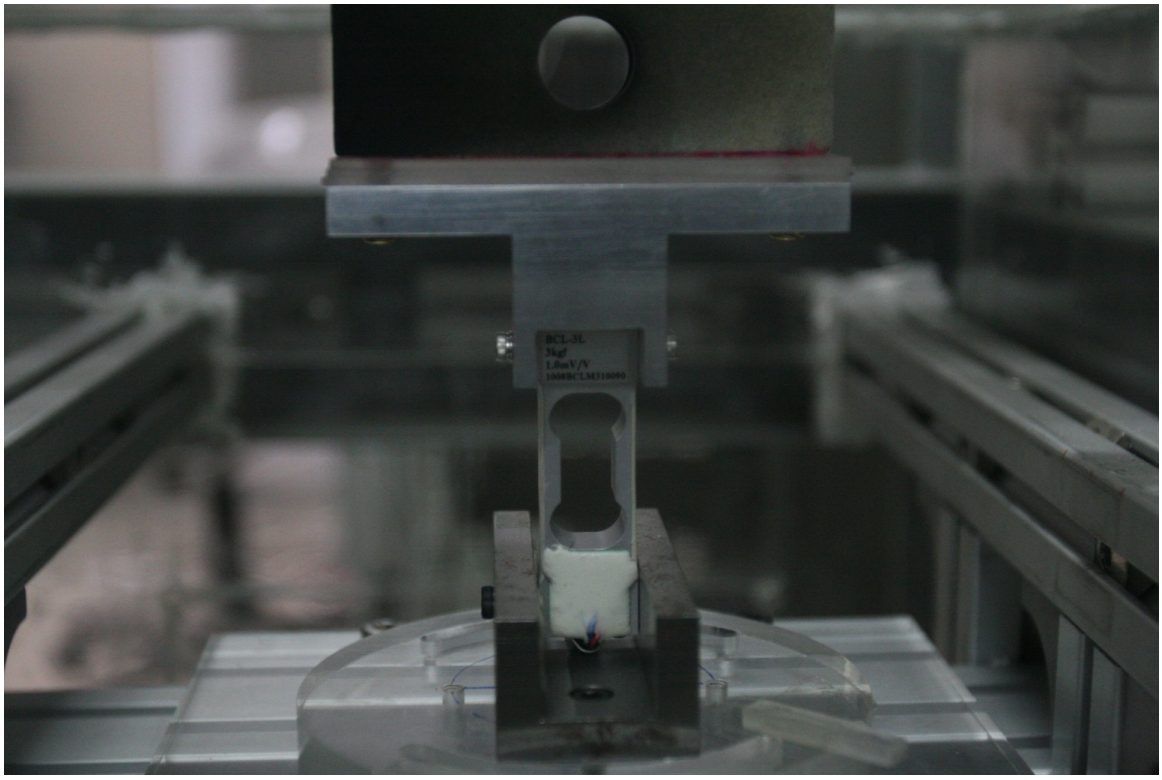

Figure 2.7. The force direct measurement system with the one axis load cell.

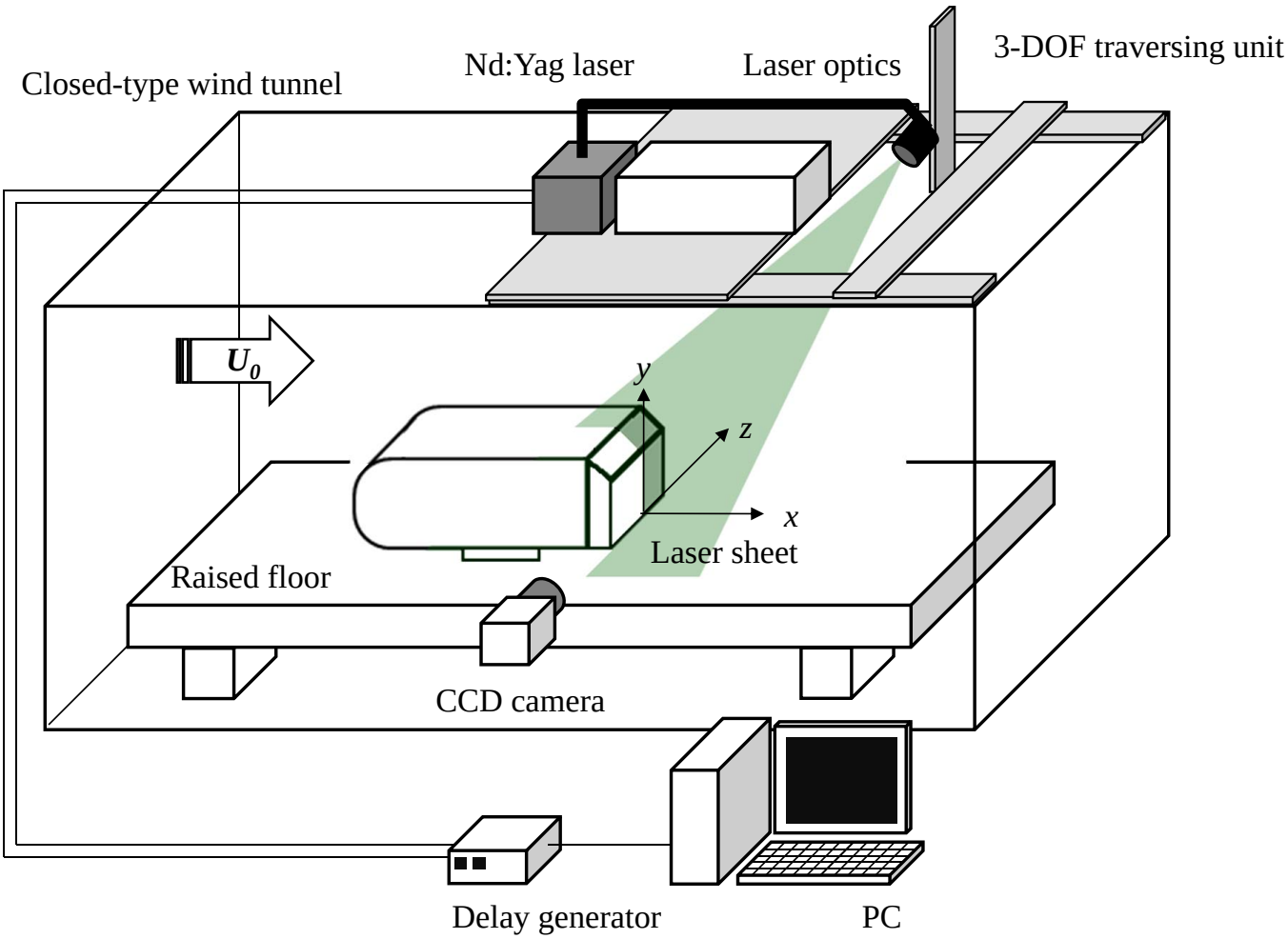

Figure 2.8. The schematic diagram of the PIV measurement system with the first field of view.

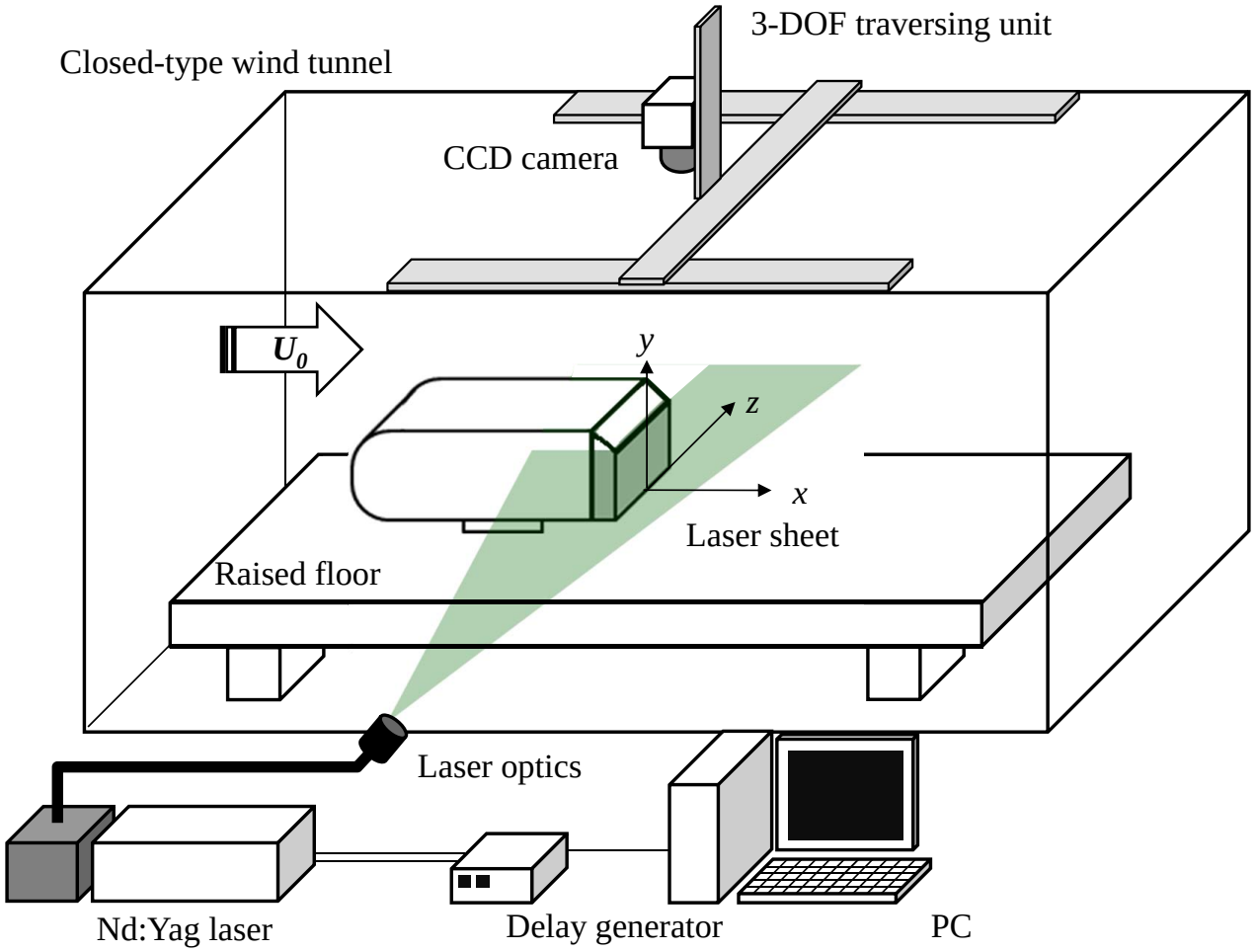

Figure 2.9. The schematic diagram of the PIV measurement system with the second field of view.

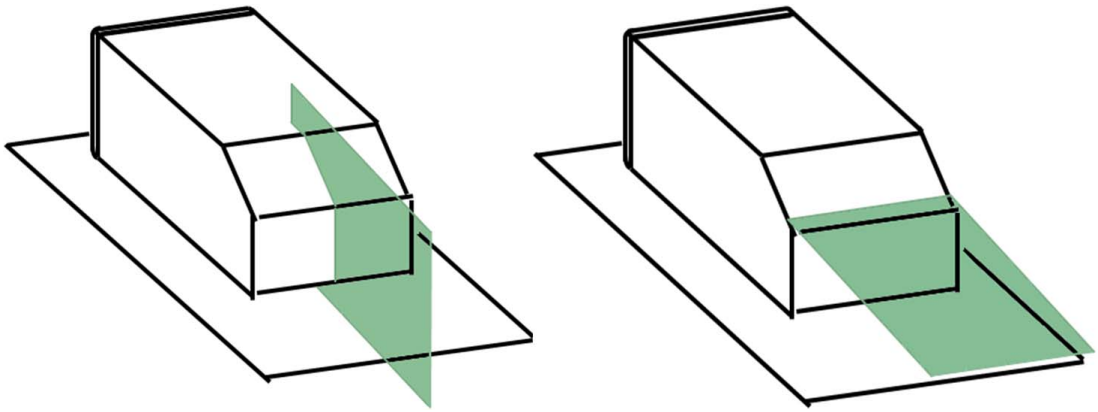

Figure 2.10. The field of views; vertical plane and horizontal plane.

Chapter 3

Results

3.1 Force measurement

3.1.1 Drag coefficient without the device

The drag on the model is measured by varying the slant angle, $\theta = 0^\circ \sim 35^\circ$, at two Reynolds numbers of 1.3×10^5 and 2.0×10^5, as shown in the figure 3.1. First of all, the drag coefficient of the original GM model ($\theta = 0^\circ$) at $Re = 2.0 \times 10^5$ is 0.3. This value well agrees with the drag coefficient measured by previous researchers (Han*et al.* (1996); Khalighi*et al.* (2001); Verzicco*et al.* (2002)). Figure 3.1 also shows that the pattern of the drag coefficient is similar to one of the Ahmed body. At $\theta = 0^\circ \sim 10^\circ$, the drag decreases with the slant angle, reaching its minimum at $\theta = 10^\circ$. With further increase in the slant angle ($10^\circ \leq \theta \leq 25^\circ$), the drag increases. At $10^\circ \leq \theta \leq 25^\circ$, main separation and two longitudinal vortices coexist on the slant surface, and these flow structures decrease the base pressure (Ahmed*et al.* (1984)). In addition, the two results from different Reynolds numbers show same tendency and this also well agrees with the explanation by (Hucho & sovran (1993)).

For the present GM model, the drag is the highest at $\theta = 25^\circ$. Although the drag of the Ahmed body is the highest at $\theta = 30^\circ$, it may be reasonable because the slant part length of the GM model is much smaller than the one of the Ahmed body; the length of the GM model is $0.3H$, on the other hand, the

one of the Ahmed body is $0.78H$. As mentioned earlier in Chapter 1, the reason for the decrease of the drag ($\theta \geq 30°$) is that the influence of the separation becomes bigger and the flow dominated by the vortices changes to another (Ahmed*et al.* (1984)). In the GM model case, the area of the slant part is so small that the influence of the separation is much bigger than the Ahmed body case, resulting in faster drag decrease.

3.1.2 Drag coefficient with the device

The performance of PMD is tested at the slant angle $\theta = 25°$, where the drag is the highest, by varying its length (h) and is shown in figure 3.2. Between $h = 10$ and 30 mm, the drag decreases more with longer PMD. However, at $h > 30$ mm, the drag no longer decreases further. Maximum drag reduction is 7.5 % at $h = 30$ mm for both Reynolds numbers. The corners of PMD are cut at a certain angle. Fixed on the PMD length (h) to 30 mm, the drag is measured with different corners, as shown in figure 3.3.

3.2 Velocity measurement

First, PIV measurements are taken in the symmetry plane of the model (Fig) with and without PMD. Figure 3.4 shows mean stream-wise velocity contours. In no control case, the flow separates from the junction between the roof and the slant surface. Once the separation starts to develop on the rear edge, the reversed flow is bound to occur on the slant surface. We also observe negative values of stream-wise velocity on the slant surface. In PMD control case, however, the position of the separation moves to the trailing edge of PMD. By means of self-lifting, PMD delays the separation point. Velocity field under PMD cannot be measured because the laser cannot reach the region

under PMD; it acts like a shade for the laser sheets. In order to investigate the wake structure, mean streamlines are calculated, as shown in figure 3.5. In the streamlines, upper recirculation core is moved away from the model by PMD, even though the length of the recirculation does not change. Because recirculation core generally indicates low pressure region, the increase of the distance between the model and the core can be considered as base pressure recovery. To support this, it should be noted that same wake modification is shown in the research of drag reduction on the square-back car model by boat tail device (Khalighi*et al.* (2001)). Attaching boat tail on the rear of the model makes the separation point transport to the extension of the boat tail, resulting in the delay of separation. Although recirculation length does not change, recirculation core is also dragged away from the body, and 20 % drag reduction is achieved.

Furthermore, velocity measurements are also taken in the horizontal plane. As shown in figure 3.6, we observe the mark of two longitudinal vortices and the loss of vortical strength by PMD. Comparing the peak values on the vortices, the strength is weakened about 25 %. The vortices structure is also one of factors of the base pressure drop, thus the weakened vortices are favorable evidence on the drag reduction.

3.3 Base pressure measurement

The base pressure is an indicator of drag force on a bluff body. Figure 3.7 shows the contours of pressure coefficient on the rear slant surface and the base region. The black solid circles denote the positions of the pressure measurement. Without PMD, strong pressure drop occurs, especially on the slant surface. This is because the flow separates from the rear edge. In contrast, the base pressure is significantly recovered with PMD. Particularly, we observe that the amount

	no control	PMD control
C_{p_b} integral (pressure tabs)	-0.286	-0.269
Pressure drag (C_{D_p})	0.302	0.285
Total drag (C_D)	0.318	0.295
The ratio of pressure drag	95.0 %	96.6 %
The ratio of pressure drag (LES)	95.0 %	

Table 3.1. Pressure drag with and without the device.

of pressure recovery is quite large on the slant surface and the upper part of the base region. This is a result from the movement of the recirculation core by means of the separation delay. In addition, the base pressure on the side edges, where two longitudinal vortices appear, is significantly recovered. It seems that the loss of the vortex strength brings pressure recovery on the side edges. To validate the pressure measurement, the pressure drag is estimated.

$$C_{D_p} = \frac{(p_f - p_b)}{\frac{1}{2}\rho U_0^2} = C_{p_f} - C_{p_b} \tag{3.1}$$

p_f and p_b are the pressures on the front and rear surface of the model vehicle, respectively. Using surface integral based on the pressure date from the tabs, C_{p_b} is obtained, as shown in the (table). However, C_{p_f} cannot be measured in the current experimental setup. Thus the integral value of $C_{p_f} = 0.016$ measured by Ahmed*et al.* (1984), considering that the fore bodies of the GM and Ahmed body are similar to each other. As shown in the table 3.1, almost 95% of total drag is the pressure drag. Even though there is limit to experimentally measure entire pressure on the surface, this ratio well agrees with LES results. Total pressure recovery ratio is 5.9 %, while it is a reasonable value considering that

drag reduction was 7.5 %.

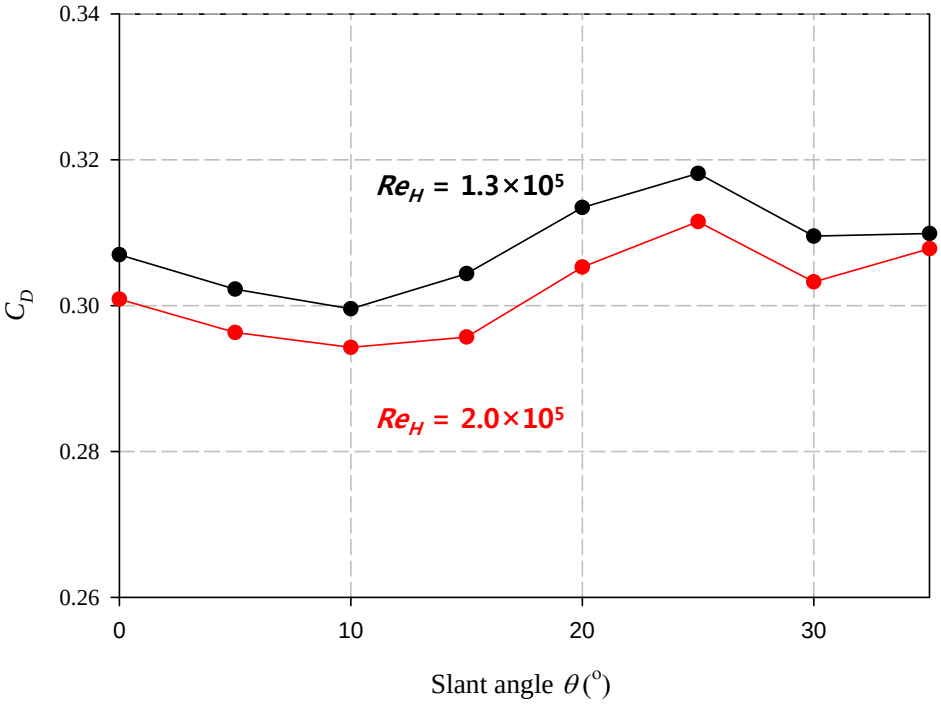

Figure 3.1. Variations of the drag coefficient with the slant angle.

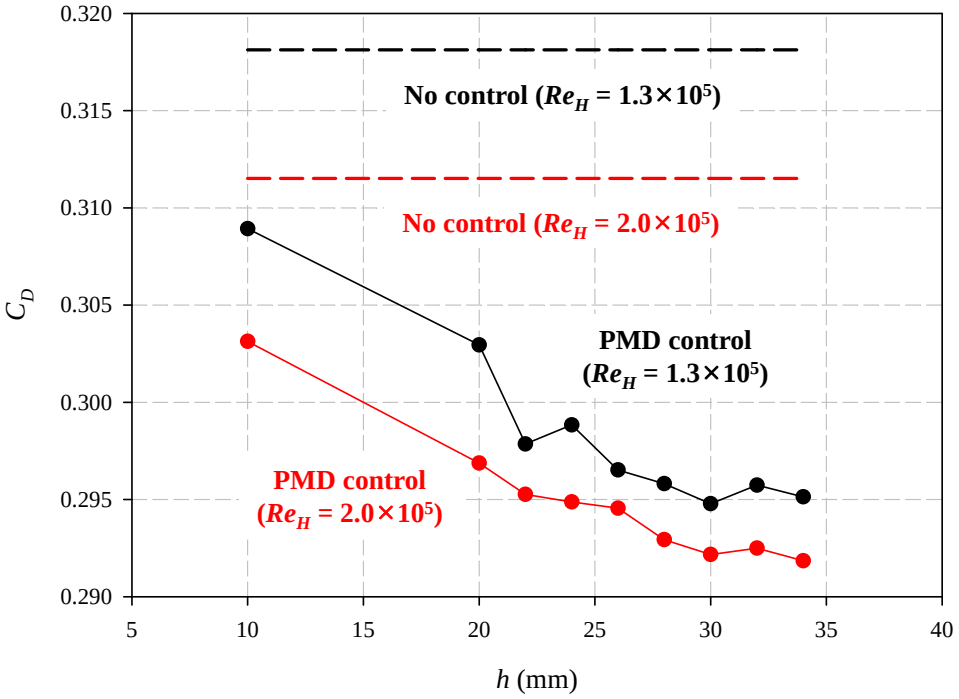

Figure 3.2. Variation of the drag coefficient with the length of PMD.

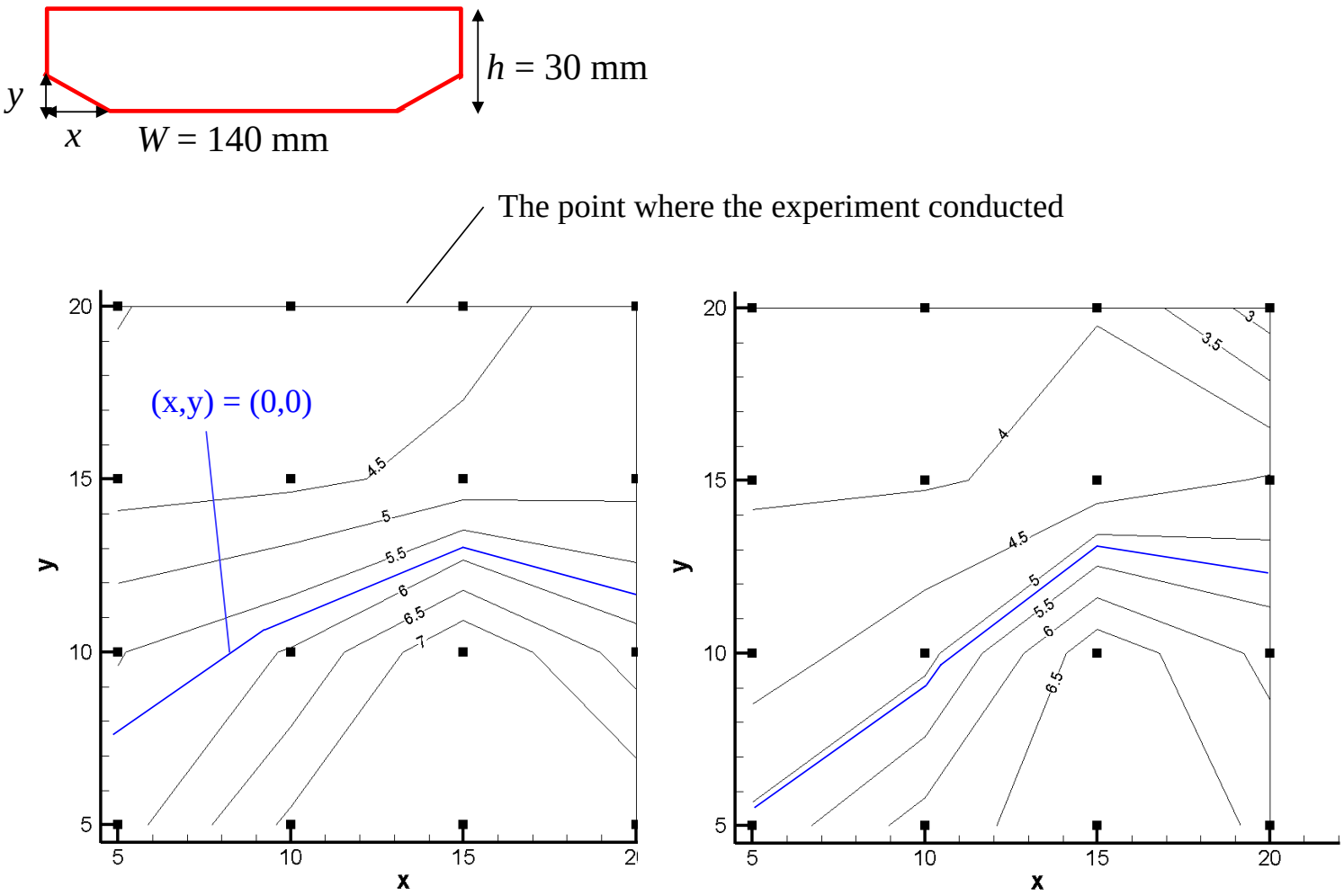

Figure 3.3. The percentage of drag reduction with the different corners.

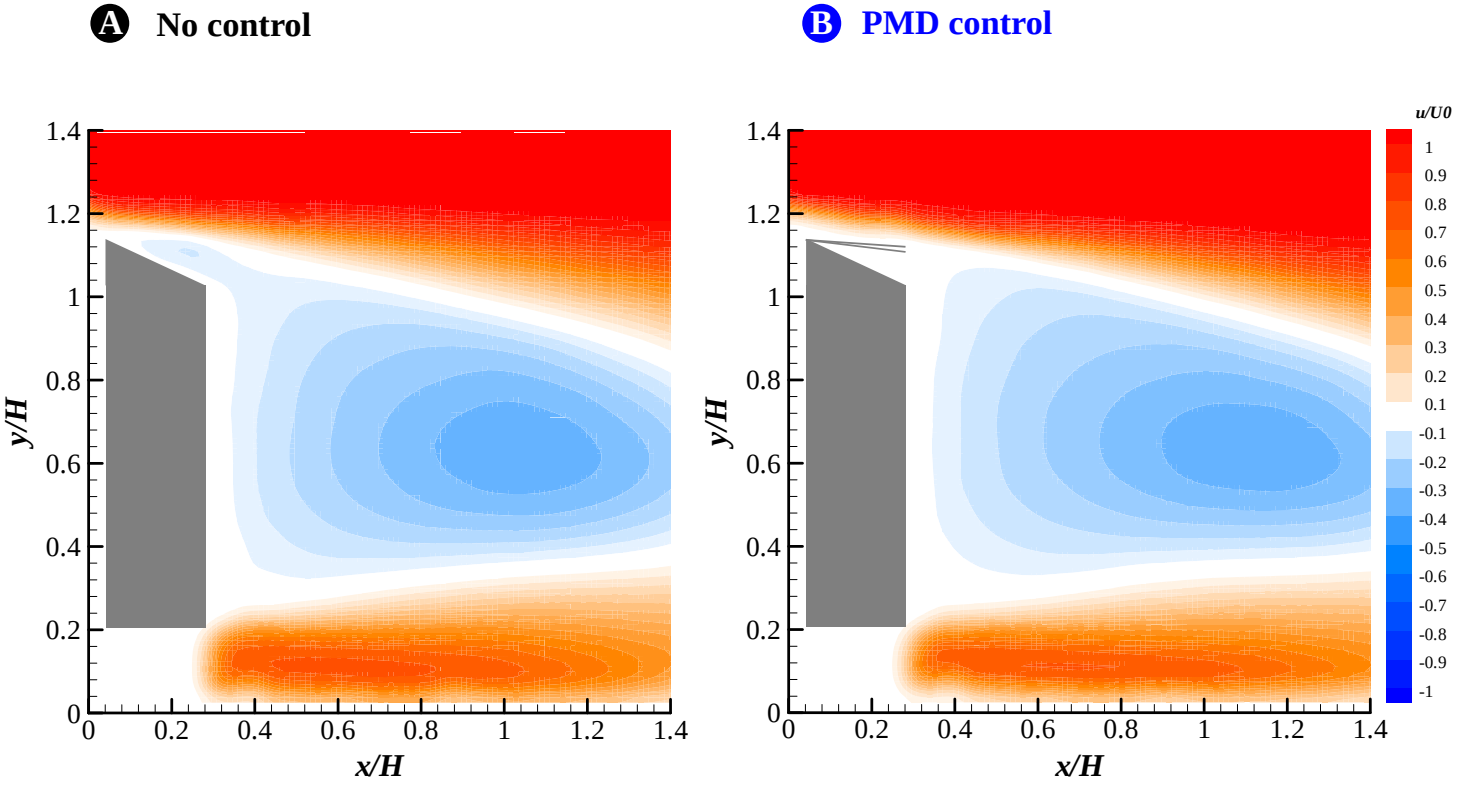

Figure 3.4. Mean stream-wise velocity contours behind the model vehicle.

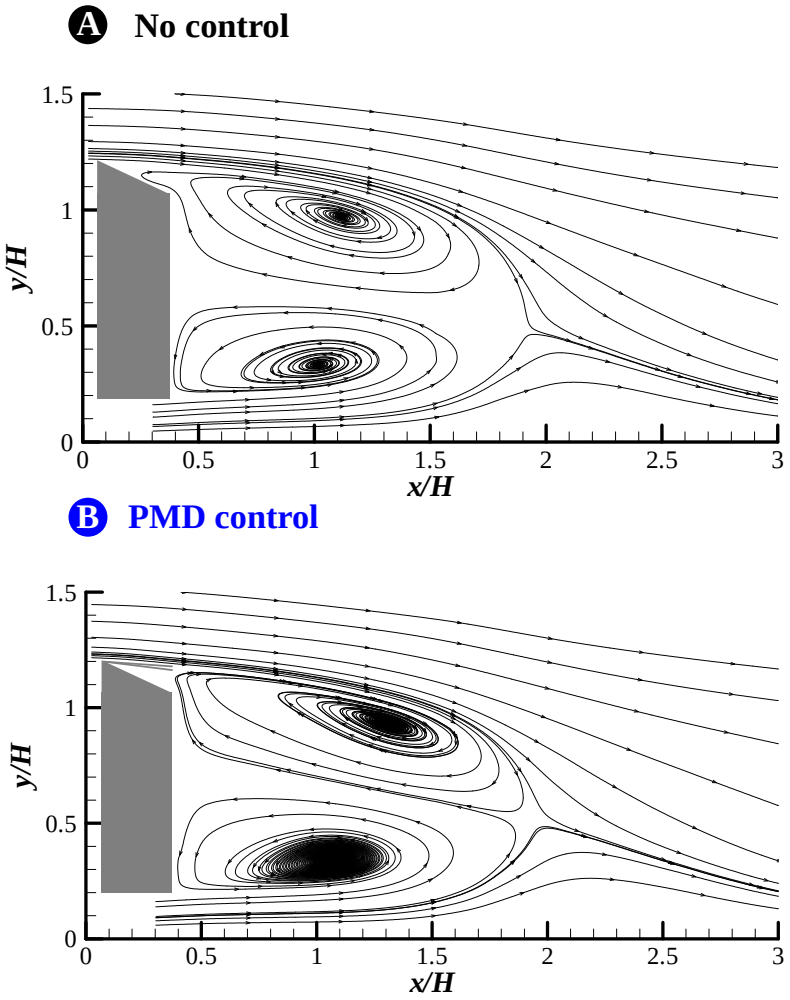

Figure 3.5. Mean streamlines behind the model vehicle.

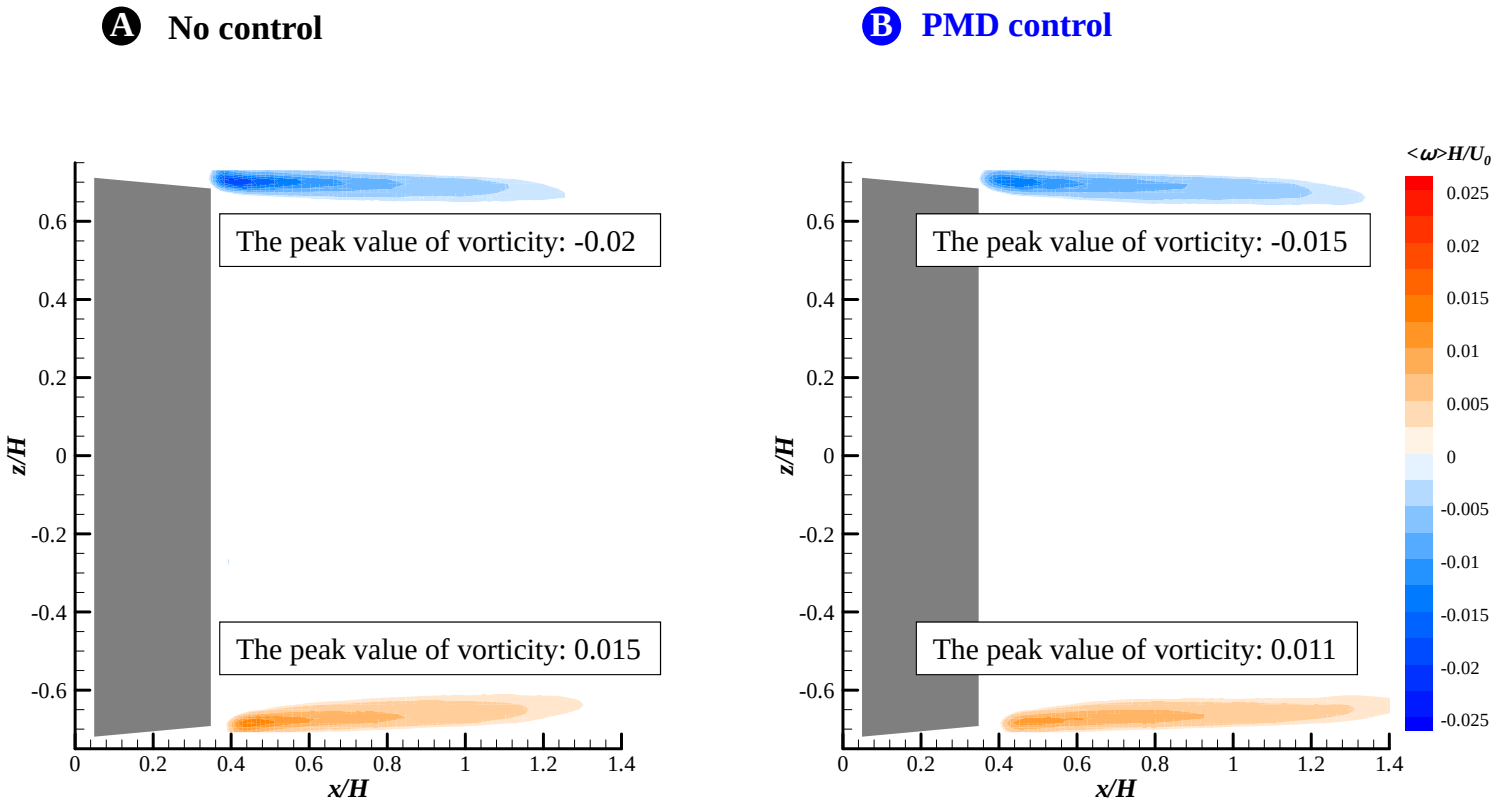

Figure 3.6. Mean vorticity contours behind the model vehicle.

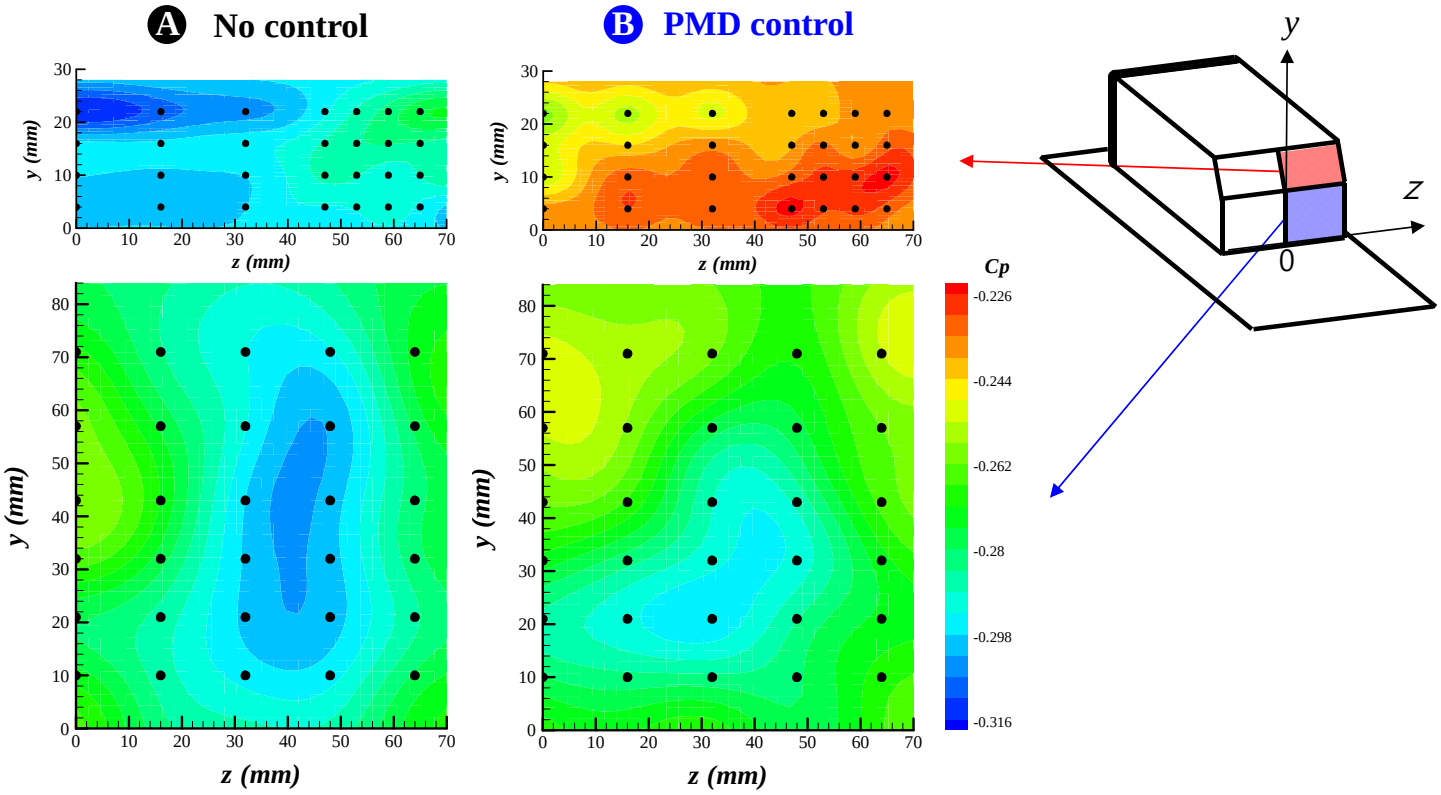

Figure 3.7. Pressure contours in base region.

Chapter 4

Summary and Conclusions

The possibility of bio-mimetic flow control was experimentally investigated for reduction of drag force on a model vehicle. The present control device (PMD) was developed from the idea that the secondary feathers on a bird's wing tend to pop up for separation delay during landing. From the present experiment, we showed that PMD makes the initial separation point to move further downstream. It increases the distance between the model and the recirculation core, which indicates low pressure field. Moreover, the two longitudinal vortices are weakened approximately 25 %. In conclusion, base pressure is recovered 5.9 %, and the drag on the model vehicle is reduced by up to 7.5 %. Moreover, PMD suggests the possibility that PMD can be applied not only the model vehicle, but also other engineering applications, such as airfoils, spheres, real vehicles and so forth.

References

Ahmed, S. R. 1981 Wake structure of typical automobile shapes *Trans. ASME: J. Fluids Eng.* **103**, 162–169.

Ahmed, S. R., Ramm, G. & Faltin, G. 1984 Some salient features of the time-averaged ground vehicle wake *SAE Paper* No. 840300.

Aider, J. L., Beaudoin, J. F. & Wesfreid, J. E. 2009 Drag and lift reduction of a 3d bluff-body using active vortex generators. *Exp. Fluids* **48**, 771–789.

Beaudoin, J. F. & Aider, J. L. 2008 Drag and lift reduction of a 3d bluff body using flaps. *Exp. Fluids* **44**, 491–501.

Bruneau, C. H. & Mortazavi, I. 2008 Numerical modelling and passive flow control using porous media. *Comput Fluids* **37**, 488–498.

Choi, H., Moin, P. & Kim, J. 1993 Direct numerical simulation of turbulence flow over riblets. *J. Fluid Mech.* **255**, 503–539.

Choi, H., Jeon, W. & Kim, J. 2008 Control of flow over a bluff body. *Annu. Rev. Fluid Mech.* **40**, 113–139.

Conan, B., Anthoine, J. & Planquart, P. 2010 Experimental aerodynamic study of a car-type bluff body. *Exp. Fluids* **50**, 1273–1284.

Fourrie, G., Keirsbulck, L., Labraga, L. & Gillieron, P. 2011 Bluff body drag reduction using a deflector. *Exp. Fluids* **50**, 385–395.

Gillieron, P. & Kourta, A. 2010 Aerodynamic drag reduction by vertical splitter plates. *Exp. Fluids* **48**, 1–16.

Han, T., Sumantran, V., Harris, C., Kuzmanov, T., Huebler, M. &

Zak, T. 1996 Flow-field simulations of three simplified vehicle shapes and comparisons with experimental measurements *SAE Paper* No. 960678.

Howard, F. G. & Goodman, W. L. 1985 Axisymmetric bluff-body drag reduction through geometrical modification *J. Aircraft* **22**, 516–522.

Hucho, W. & Sovran, G. 1993 Aerodynamics of road vehicles *Annu. Rev. Fluid Mech.* **25**, 485–537.

Khalighi, B., Zhang, S., Koromilas, C., Balianyi, S. R., Bernal, L. P., Iaccarino, G. & Moin, P. 2001 Experimental and computational study of unsteady wake flow behind a bluff body with a drag reduction *SAE Paper* No. 2001-01-1042.

Liebe, W. 1979 Der Auftrieb am Tragugel: Entstehung und Zusammenbruch. *Aerokurier* **12**, 1520–1523.

Lienhart, H., Stoots, C. & Becker, S. 2003 Flow and turbulence structures in the wake of a simplified car model *SAE Paper* No. 2003-01-0656.

McCallen, R., Couch, R., Hsu, J., Leonard, A., Brady, M., Ross, J., Stroms, B., Heineck, J. T., Driver, D., Bell, J., Zillizc, G., Browand, F., Hammache, M., Salari, K. & Rutledge, S. 1999 Progress in reducing aerodynamic drag for higher efficiency of heavy duty trucks (Class 7-8) *SAE Paper* No. 1999-01-2238.

Mohamed-Kassim, Z. & Filippone, A. 2010 Fuel savings on a heavy vehicle via aerodynamic drag reduction. *Transportation Research Part D* **15**, 275–284.

Ortega, J., Salari, K. & Storms, B. 2009 Investigation of tractor base bleeding for heavy vehicle aerodynamic drag reduction. *The Aerodynamics of Heavy Vehicles : Trucks, Buses, and Trains* **41**, 161–178.

Spohn, A. & Gillieron, P. 2001 Flow separations generated by a simplified

geometry of an automotive vehicle. *In: UTAM Symposium on unsteady separated flows, Toulouse, France*

Verzicco, R., Fatica, M., Iaccarino, G. & Moin, P. 2002 Large eddy simulation of a road vehicle with drag reduction devices *AIAA* **40**, 2447–2455.

Walsh, M. J. 2009 Turbulent boundary layer drag reduction using riblets. *AIAA., Aerospace sciences meeting, 20th, Orlando, FL, Jan* 11–14.

생체 모방 유동 제어를 통한 3 차원 자동차 모델의 항력감소

서울대학교 대학원
기계항공공학부
이 훈

요약

본 연구에서는 생체모방을 이용해 새로운 유동 제어 장치를 개발하고, 그 장치를 사용해 3 차원 자동차 모델의 항력감소를 이루어냈다. 또한 자동차모델이 받는 힘, 주위의 압력과 속도를 측정함으로써 새로운 항력 감소장치의 메커니즘을 분석했다.

새의 날개 위 깃털은 평상시에는 날개 위에 붙어 있다가, 날개 끝단에 유동박리가 발생할 때 유동박리의 역류에 반응해 들리게 되고, 깃털이 들림으로써 유동박리의 확장을 막는다. 자동차의 경우도 자동차 후면의 기울어진 영역에서 발생하는 유동박리가 항력의 주된 원인 중 하나이기 때문에, 새의 깃털을 모사한 장치가 유동박리의 효과를 억압할 수 있다고 판단, 깃털을 모방한 장치에 대한 연구가 수행되었다. 새로운 장치는 유동박리가 발생하지 않는 낮은 유속에서는 자동차 후면에 붙어 있다가, 유동박리가 발생하면 역류에 반응해 스스로 움직여 유동박리를 억압한다. 이 스스로 움직이는 장치를 통해 최대 7.5 %의 항력감소를 이루어냈다. 압력 탭과 PIV 를 이용해 자동차 후면의 압력, 속도장을 측정한 결과, 낮은 압력을 야기하는 유동박리가 PMD 에 의해 모델에서부터 멀어지게 되었고 이에 따라 압력이 회복되어 항력이 감소한 것으로 분석되었다.

주요어: 3 차원 차량 모델, 항력 감소, 유동 제어, 생체 모방

학번: 2010-24070

감사의 글

안녕하세요. 올해 8 월에 졸업하는 이 훈 입니다. 논문 작성을 끝마치고 감사의 글을 쓰려고 하니, 제가 처음으로 서울대학교의 최해천 교수님 연구실을 찾아 갔을 때가 가장 먼저 생각이 납니다. 정문 안으로 들어서는 순간 여기가 산인지 학교인지 분간할 수 없었고, 어느 버스를 타서 어느 정류장에 내려야 301 동 이란 곳에 갈 수 있는지도 몰랐으며, 캠퍼스 안에 있는 사람들이 너무 낯설게 느껴졌습니다. 하지만 2 년이 지나고 보니, 학교 안의 모든 버스 노선들을 완벽히 파악하고, 학교에서 먹고 자며 캠퍼스와 동화된 저를 발견할 수 있었습니다. 시간은 정말 쏜살같이 흐르나 봅니다.

제일 먼저 저를 받아주시고 연구를 지도해주신 최해천 교수님께 감사 드립니다. 교수님과 함께 연구를 하고 미팅을 진행하면서, 교수님이 얼마나 유명하신 분인지 그리고 왜 유명하게 되셨는지를 알게 되었습니다. 연구와 관련된 가르침도 많이 받았지만, 틈틈이 연구 외적인 가르침도 많이 받았습니다. 부족한 저를 2 년 동안 지도해 주셔서 감사합니다. 2 년전 교수님을 처음 찾아 뵈었을 때 교수님은 일본에서 온 저를 따뜻하게 받아주시고 잘 할 수 있을 거라며 저를 격려해 주셨습니다. 제가 낯선 이곳에서 잘할 수 있을까라는 두려움이 많았는데, 교수님과 면담하면서 두려움이 많이 없어졌습니다. 잘할 수 있다라는 자신감이 생겼었습니다. 저의 연구실 생활은 교수님과의 첫 면담을 계기로 시작된 것이나 다름 없습니다. 졸업할 때가 되고 나니 잘한 점 보다는 잘못한 점이 많이 생각납니다. 부족한 학생이었지만 사회에 나가서 교수님의 가르침 잊지 않고 열심히 살겠습니다.

그리고 저를 낳아주시고 키워주신 부모님께 감사 드립니다. 장남인데도 불구하고 장남 노릇 못하는 못난 아들 열심히 키워주셔서 감사합니다. 고등학교를 졸업하자 마자 집을 떠나서 유학생활을 하다 보니, 부모님께서 오랫동안 적적해 하셨을 거 같습니다. 유학을 끝마치고 한국에 와서도 연구실 일이 바빠서 집에 오래 붙어있지 못했습니다. 이제 드디어 졸업하나 했더니 곧 취직해 지방으로 떠나니, 저는 불효 자식이 아닐 수 없습니다. 하지만 방학 시즌에 귀국할 때 마다 공항까지 나와 반겨주셨던 부모님, 아무리 졸리셔도 아침 꼬박꼬박 챙겨주시는 부모님, 옷 정리 해라 방 정리해라 나중에 결혼해서 마누라한테 무슨 소리 들으면서 살거니 라며 제 결혼생활까지 걱정해 주시는 부모님. 항상 잊지 않고 있습니다. 앞으로 더욱 효도하겠습니다. 하나뿐인 여동생 지연이. 내가 오빠지만 사실 네가 더 어른스럽고 철이 들은 거 같다.

그래서 우리 사이가 친구 사이 같이 편한 걸 수도 있겠지. 부모님 잘 챙겨드리고 직장생활 열심히 하길 바래. 우리 집 고양이 유키. 비록 이 글을 너가 볼 수는 없겠지만, 내가 밤늦게 들어오든 새벽에 들어오든 아침에 들어오든 매일 매일 졸린 눈으로 나한테 와서 이제 왔냐며 말을 걸고 쿨하게 돌아서는 너를 잊지 않고 있다. 항상 고맙다.

TFC 연구실 생활을 함께 했던 모든 사람들에게도 감사의 인사를 합니다. 제일 먼저 주하형께 감사의 말씀을 드리고 싶습니다. 중요한 발표, 학회, 디펜스 전에 항상 저희와 함께 밤새가며 도와주셨던 주하형, 감사합니다. 제가 연구, 인간관계, 혹은 여자친구 관계로 힘이 들 때 주하형이 해주신 조언이 아직도 기억에 남습니다. 가끔 버릇없는 후배였지만 애교로 봐주시고, 틈틈이 연구실을 찾아 뵙겠습니다. 실험실의 살림살이를 도맡아 하시는 홍권이형, 형이 없었다면 저는 졸업할 수 없었을 거 같습니다. 평소에 연구, 학부생 지도에 관한 많은 조언을 받았습니다. 하지만, 정말 중요하지만 대부분 중요하게 생각하지 않는, 공구들의 위치, 사용법, 안전장비의 필요성 등의 대부분을 형에게 배웠습니다. 형이 계시기 때문에 실험 팀 사람들은 편하게 실험을 할 수 있는 거 같습니다. 저에게 필름카메라의 길을 열어주셨던 지훈이형, 정일이형 감사합니다. 근엄하시고 인자하신 정일이형, 나이 차이는 나지만 뭐든지 터놓고 얘기할 수 있었던 지훈이 형, 두분 다 항상 행복하시고 하는 일 잘 되셨으면 좋겠습니다. 14 층 방장님 이시자 제 옆자리에 앉으시는 의영이형, 정밀연 간다고 옆자리를 지켜드리지 못해 죄송합니다. 매일매일 누구보다 일찍 와서 누구보다 늦게 가는 형이 존경스럽습니다. 항상 솔직하시고 재미있으신 태용이형, 남은 박사과정 즐겁게 보내시길 바랍니다. 털이 많은 인재형, 저희가 놀려도 다 장난으로 받아주시고, 제가 시도 때도 없이 질문해도 항상 답해주셔서 정말 감사했습니다. 요즘 건강이 안 좋으시다고 들었는데 건강 잘 챙기시길. 귀염둥이 동건이형, 재미있을 땐 재미있고, 진지할 땐 진지한 형이 좋습니다. 송도 학회 때 형에게 많은 조언을 받았던 것도 생각이 납니다. 좋아하는 게임도 비슷한데 조만간 또 만나요. 나보다 선배인 우진이와 현식이, 같이 술 마시고 수다 떨고 항상 붙어 다니던 사이인데 어느덧 헤어질 때가 되었구나. 박사과정 즐겁고 편안하게 마무리 했으면 좋겠다. 세상에서 가장 소중한 저희 동기들, 종오형, 재명이, 윤식이. 한국에 와서 힘이 들 때 마다, 그래도 내가 얻은 보물이 있다면 이 3 명의 동기라고 항상 생각했습니다. 길게 얘기하지 않겠습니다. 자주 모입시다. 후배지만 선배 같은 지은이, 학회, 디펜스 때마다 너무 많은 도움을 받았다. 고마워. 너라면 편하게 졸업할 수 있을 거야. 하는 일 다 잘되길 바랄게. 항상

재미있고 술잘마시는 훈재, 쿨가이 창원이, 고궁을 좋아하는 민욱이, 301 동 퀸카 민정이, 농구 잘하는 창우, 팀이 달라서 많은 얘기를 나누지는 못했지만 너네 들은 누구보다 착한 후배였고 앞으로 연구실 생활도 잘할 거라 믿는다. 실험 팀 후배 경태, 기쁠 때나 슬플 때나 함께 있어줘서 고마워. 연구실 들어오자 마자 내 실험 셋팅도 많이 도와주고 넌 정말 착한 후배였다. 꼭 창원에 놀러 오렴. 실험 팀 형님들인 희수형, 승현이형, 같이 운동하고 수다 떨던 시간들이 그리워 질 거 같아요. 졸업하고 나서도 자주 찾아 뵙겠습니다. 수치 팀 막내 기영이, 너는 똑똑하고 성실해서 뭐든 잘 해낼 거 같아. 지금처럼만 열심히 하렴. 마지막으로 중대장님 은혜, 만난 시간은 짧지만 재미있는 일이 많았던 거 같아. 앞으로 어렵고 힘든 일이 많이 생기겠지만 그럴 때 마다 다시 한번 힘을 내길 바라고 항상 건강하렴.
그리고 내 동네 친구들. 같은 아파트 사는 한준이, 도윤이, 덕수, 지웅이, 지수. 서울 생활 하면서 자주 만나는구나. 힘들고 지칠 때 마다, 너네 들이 동네에 있어서, 언제든지 편하게 만나고 얘기할 수 있어서 나에겐 정말 많은 도움이 됐어. 우리 우정 변치 말고 영원하자.
동아리 후배들, 수진이, 유미, 태영이, 승희, 나원이. 연구실 바깥에서 만나게 된 유일한 동생들아. 워낙 똑똑하고 밝은 너네 들을 보면 나의 나이를 실감한단다. 가끔 밥 사주러 학교에 올 테니 변치 않고 있으렴.
이렇게 하나 하나의 인연을 생각하니 저는 정말 복 받은 사람이란 생각이 듭니다. 이 인연들 끊기지 않도록 노력하겠습니다. 저의 석사과정 동안 저라는 부족한 사람과 인연을 맺어주신 모든 분들께 감사의 마음을 전합니다. 일본에는 이런 말이 있습니다. 진정한 고마움이란 고맙다 라는 말로는 부족하다. 말로만 고맙다고 하는 사람이 아닌, 행동으로 보여주는 사람이 되겠습니다. 2 년 동안의 서울대 생활을 함께한 모든 분들, 저에게 큰 보배입니다. 항상 건강하세요!

2012 년 6 월 29 일
여느 때와 다름없이 정밀연 312 동 303 호에서
이 훈 올림.